



Using Statistical Shape and Appearance Modelling to characterise the 3D shape and material properties of human lumbar vertebrae: A proof of concept study

G.A. Day^{*}, A.C. Jones, R.K. Wilcox

Institute of Medical and Biological Engineering, Mechanical Engineering, University of Leeds, UK

ARTICLE INFO

Keywords:

Finite element
Statistical shape and appearance model
Statistical shape model
Shape model
Vertebra
Spine

ABSTRACT

Patient variation affects the outcomes of a range of spinal interventions, from disc replacement to vertebral fixation and vertebroplasty. Statistical Shape and Appearance Modelling (SSAM) can be used to describe anatomical variation and pathological differences within the population. To better understand how bone density and shape variation affect load transfer with respect to surgical treatments, Finite Element (FE) models can be generated from a SSAM. The aim for this study is to understand whether geometric and density variation as well as multiple vertebral levels can be incorporated into a single SSAM and whether this can be used to investigate the relationships between, and effects of, the various modes of variation.

FE models of 14 human lumbar vertebrae that had been μ CT imaged and validated through experimental testing were used as input specimens for a SSAM. The validity of the SSAM was evaluated by using principal component analysis to identify the primary modes of geometric and bone density variation and comparing to those in the input set. FE models were generated from the SSAM to examine the response to loading.

The mean error between the input set and generated models for volume, mean density and FE compressive stiffness were 10%, 3% and 10% respectively. Principal Component (PC) 1 captured the majority of the bone density variation. The remaining PCs described specific geometric variation. The FE models generated from the SSAM showed the variations in vertebral stiffness as a result of complex relationships between bone density and shape.

The SSAM created has limited data for its input set, however, it acts as a proof of concept for the novel combination of material and shape variation into a single shape model. This approach and the tools developed can be applied to wider patient groups and treatment scenarios to improve patient stratification and to optimise treatments.

1. Introduction

Low back pain is reported to be the fourth leading cause of disability adjusted life years globally (Hurwitz et al., 2018) and while many patients with lower back pain respond to conservative treatments, approximately 22% require more invasive and expensive interventions such as arthrodesis, arthroplasty and vertebroplasty (Dagenais et al., 2008). Both the geometric and density variation found within the vertebrae have large effects on the efficacy of a range of treatments. Changes to the bone density and its distribution throughout the vertebral body have implications for the treatment of vertebral fractures through cement augmentation (Day et al., 2020; Aquarius et al., 2014),

as well as influencing the subsidence risk for intervertebral disc treatments such as fusion cages (Hasegawa et al., 2020) and total disc replacements (De Beer and Scheffer, 2012).

Statistical shape and appearance models (SSAM) give the opportunity to investigate the modes of variation in a dataset that would otherwise be difficult to isolate. Here, the appearance refers to the material density of the specimens and specifically the distribution of that density throughout the volume. In the case of vertebrae, the relationship between various geometric measurements, the density and its spatial variation through the vertebra all have a complex and interlinked effect on the response to both in-vivo loading and treatments alike. To understand the effect of these variables either experimentally or

^{*} Corresponding author.

E-mail address: g.day1@leeds.ac.uk (G.A. Day).

<https://doi.org/10.1016/j.jmbbm.2021.105047>

Received 5 August 2021; Received in revised form 8 December 2021; Accepted 11 December 2021

Available online 15 December 2021

1751-6161/© 2022 The Authors. Published by Elsevier Ltd. This is an open access article under the CC BY license (<http://creativecommons.org/licenses/by/4.0/>).

computationally using specimen specific models, a large range of vertebrae with varying shapes and properties would be required to represent the range in the population. Even if this could be achieved, confounding factors and other variation would make the presentation of specific relationships difficult. Using statistical shape and appearance models with principal component analysis (PCA), the modes of variation can be characterised and isolated, allowing an understanding of how specific modes of variation affect the chosen measure.

The general aims of most statistical shape (and appearance) models in this field have been to describe the geometric variation of bones across a sample population. This is usually carried out by comparing the mean of the sample group to the main modes of variation found within it (Clogenson et al., 2015). Such approaches have been used to characterise shape variation in the cervical spine (Bredbenner et al., 2014), pelvis (Meller and Kalender, 2004), clavicle (Lu and Untaroiu, 2013) and femur (Nicolella and Bredbenner, 2012; Bryan et al., 2010), amongst others. In the lumbar spine, studies have used statistical shape models to identify the variation both in spinal curvature (Ali et al., 2012; Meakin et al., 2009, 2013; Boisvert et al., 2008; Campbell and Petrella, 2015, 2016; Hollenbeck et al., 2018) and single vertebrae (Hollenbeck et al., 2018). However, these tools have yet to be applied to examine the shape and density distribution together for vertebrae.

The primary aim of this study was to prove the novel concept for the incorporation of multiple vertebral levels, shape and material variation into a single statistical model, which can then be expanded to larger datasets to understand variation in the population. The first objective was to generate a SSAM to represent the variation in a set of lumbar spinal vertebrae, and assess its efficacy by comparing the resulting models to the input set specimens. The second objective was to analyse the novel incorporation of shape and density variation together, and assess how these combined variations affect the vertebral stiffness under different loading positions. Detailed below is the process of creating the SSAM, the methodology used to assess and characterise the variation found in the generated models and the outcomes of applying load to the models.

2. Materials and methods

2.1. Specimen provenance and selection

Fourteen human lumbar vertebral bodies were harvested from four cadaveric spines obtained with ethical permission from the Leeds GIFT Research Tissue Project, as detailed in Table 1.

2.2. Experimental testing, imaging and FE model generation

The mechanical testing and specimen-specific finite element modelling of the specimens was reported previously by Day et al. (2020). Briefly, all specimens were potted in PMMA endcaps and imaged using a HR-pQCT (XtremeCT, Scanco Medical AG, Switzerland) at an isotropic voxel size. Each vertebra was placed between two steel end-plates and loaded under axial compression in a materials testing machine (Instron 3366, 10 kN load-cell, Instron Ltd, UK) to 1600 N. The stiffness of each vertebra was measured by identifying the maximum gradient on the load displacement curve.

Finite element models that matched the experimental specimens were created, following the methodology described by Day et al. (2020).

Table 1

Details of the lumbar sections used from four cadaveric spines.

Spine Name	Vertebrae	Sex	Age
Spine 1	L1, L2, L3, L4, L5	F	90
Spine 2	L1	F	94
Spine 3	L1, L2, L3	M	86
Spine 4	L1, L2, L3, L4, L5	M	83

The models consisted mainly of 1 mm³ hexahedral elements with tetrahedral elements used on the model surfaces to allow more accurate FE contacts and description of the shape. Element-specific material properties were applied to the bone, which were linearly correlated to the local bone density, derived from μ CT image data, with an experimentally calibrated constant. This constant was derived by using an optimisation process (Mengoni, 2017; Mengoni et al., 2015), in which the value was sequentially altered until the best agreement was found between the FE model predictions of stiffness and the corresponding experimentally-measured values. The PMMA cement in the endcaps was assigned a Young's modulus of 2.45 GPa and a Poisson's ratio of 0.3 (Day et al., 2020; McCormack et al., 1994). These FE models were solved under conditions that mimicked the experimental loading procedure to obtain their stiffness using Abaqus (2017, Dassault Systèmes, France). The predicted stiffness values of the computational models were found to match well to the corresponding experimental values (Concordance Correlation Coefficient = 0.86).

2.3. Statistical shape and appearance model creation

A bespoke plugin for Simpleware ScanIP (Synopsys, USA) was developed in collaboration between the authors and the software manufacturers and was specifically designed for the analysis of vertebrae. This tool was used to generate and analyse the SSAM and follows similar steps to other statistical shape modelling workflows (Clogenson et al., 2015; Lu and Untaroiu, 2013; Yates et al., 2016; Grassi et al., 2014). An overview of the workflow is shown in Fig. 1. The tool utilises the Insight Tool Kit (ITK (McCormick et al., 2014),) to generate the SSAM model based on an input set of bone geometries (masks) overlaid with CT-based density distribution maps (background images), created in Simpleware ScanIP. The process was carried out in five main steps. (i) Pre-processing

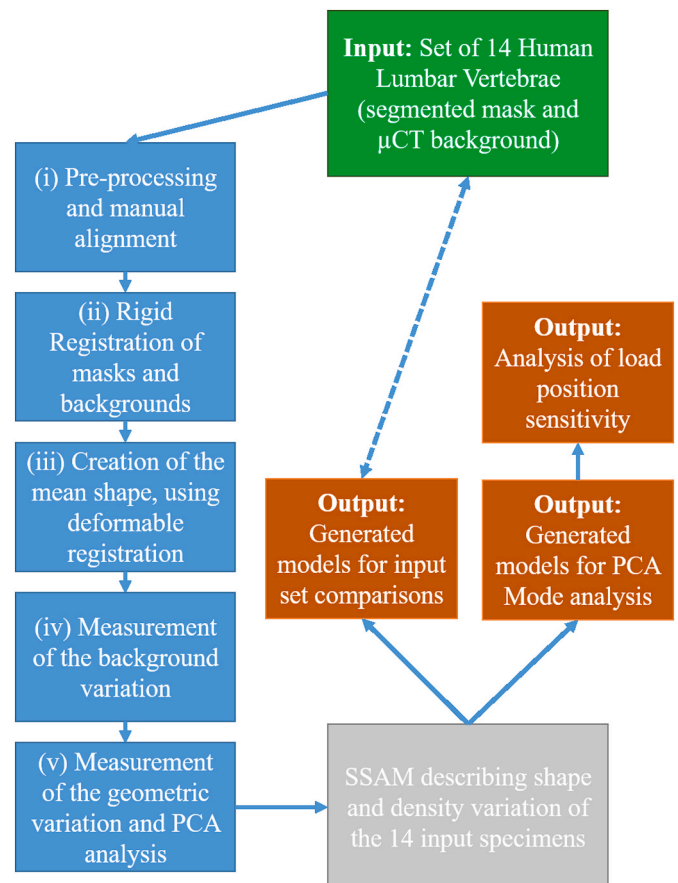


Fig. 1. Flow chart describing the SSAM creation.

was first undertaken to convert the masks and background images into necessary formats (.mha & .mhd) for use with the ITK tool-kit. The masks and backgrounds of each vertebra were manually aligned such that the vertebrae were centred and the average of plane of the vertebral endplates was parallel to the horizontal. (ii) Rigid registration of the models was performed, aligning the masks and backgrounds to a shared coordinate system. This step was carried out using the ITK library with the registration being measured according to a mean squared image-to-image metric using a gradient descent optimiser. (iii) The mean shape was determined by describing the geometry of each input specimen in a deformable registration step, by measuring the transform required to morph the mean of the input set onto each of the other input models until a minimum was found using the ITK FEM registration filter. This deformation based statistical shape modelling approach removed the need for correspondence points found in many other studies (iv) The density distribution of the input models were described by the difference between the greyscale value of each voxel from the input set to the greyscale value of the corresponding voxel on the mean model. To allow the greyscale variation to be calculated, the background of each input model was first morphed through the same deformable registration transform that each input model underwent to capture the geometric variation (from step iii). The change of each voxel's greyscale value from each model could then be measured and added to the geometric variation to describe the total variation of each model. (v) The transforms between the mean and each of the input vertebrae are used to describe the vertebral geometries. These, along with the differences in voxel greyscale values, were used as inputs for the PCA. The outputs of this step included the principal components, their eigenvalues, the proportion of variation captured in that component and the cumulative proportion of variation captured.

Following these steps, new models formed of mask and background combinations were generated using the ITK Image Warp filter. The first three principal components, which represented the majority of the overall variation, were varied and used to generate models from the SSAM.

2.4. Comparison of vertebral variation to the input set

Comparisons of the vertebral properties were carried out for the geometric, density and stiffness measurements. In each case, the data obtained across the input set of models was compared to a generated set of models describing all possible variation within 1 S.D. of the mean from the first three principal components. The 15 models, with their modal variation are shown in Table 2. Models with larger standard deviations from the mean were not tested here given that their trends would have been the same as for the ± 1 S.D models but with greater magnitude.

2.4.1. Geometry

To compare the shape of the models generated from the SSAM to the input models, broad measures of the vertebral geometry were made similarly to Hsu et al. and Hollenbeck et al. (Hollenbeck et al., 2018; Hsu et al., 2019). This was achieved in an automated fashion by fitting regular cuboids around a point cloud describing each of the generated and input models. Three cuboids were fitted on each of the three anatomical planes (Fig. 2 shows the three axial cuboids). The two long

sides of the nine fitted cuboids were measured to give 18 dimensions that described most aspects of vertebral geometry (Fig. 2). In addition to the 18 vertebral measurements, the mean and range of vertebral volumes were also compared.

2.4.2. Greyscale appearance

Variation in the density was analysed by calculating the mean greyscale value for each vertebra, and comparing the mean and range of those values between the generated and input sets. Details of density distribution were compared through greyscale histograms of two sets.

2.4.3. Stiffness

The model stiffness was examined by meshing the generated vertebrae and applying loads in FE that mimicked those applied to the input set and experimental specimens (Day et al., 2020). The same experimentally-calibrated constant for the element specific material properties was used as described above.

In order to make comparisons with the specimen-specific models, PMMA endcaps (6 mm total depth, 90 mm diameter) were also added to each generated model using a script within the ScanIP Python environment. The material properties for the cement and bone matched those for the specimen specific models. The models were solved under the same boundary conditions and loads as the specimen-specific models.

Comparisons were made between the range and mean stiffness of the generated models and the input model stiffness values.

2.5. Analysis of modes of variation using finite element models

In order to investigate the mode of variation captured by each principal component, models were created at ± 1 , ± 2 and ± 3 standard deviations away from the mean for the first three principal components independently. Exact details are available in the associated dataset (Day et al., 2021). The mean model was also generated, as a baseline for comparison. The greyscale distribution, FE density distribution, stiffness and modes of shape variation were measured and compared.

2.6. Analysis of variation and load position sensitivity

The sensitivity of the generated models to being loaded anteriorly and posteriorly was tested. This allowed an investigation into how the modes of variation affected different loading scenarios. Load positions were at 10 mm and 20 mm posterior and anterior of the central loading position, generally corresponding with the anterior and posterior walls of the vertebral body at 20 mm, shown in Fig. 3.

3. Results from the generated models

The data set associated with this paper is openly available from the University of Leeds data repository (Day et al., 2021).

Results from the principal component analysis of the input set show that 72% of the variation within the dataset was captured in the first five principal components. The weighting of the first five PCs is shown in Table 3.

Table 2

Standard deviations of the models generated to compare the geometric, density and stiffness variation. The vertebrae should describe all possible variation within 1 S.D of the mean for the first three principal components. 0 describes the mean position for the principal component and the 0,0,0 vertebrae represents the overall mean model.

Mode of Variation	Model Description in Terms of Mode Combination														
PC1	0	-1	1	0	0	0	0	1	-1	1	-1	1	-1	1	-1
PC2	0	0	0	-1	1	0	0	1	1	1	1	-1	-1	-1	-1
PC3	0	0	0	0	0	-1	1	1	1	-1	-1	-1	-1	1	1

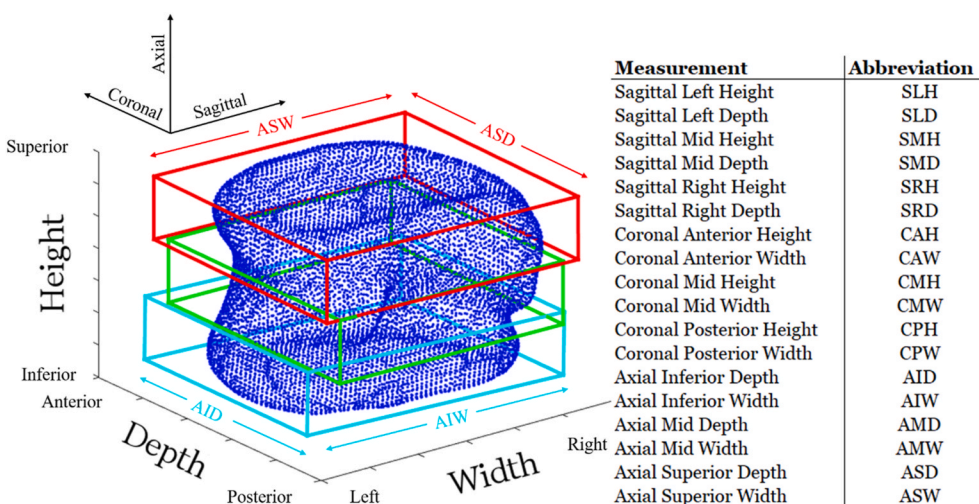


Fig. 2. An example of the vertebral measurement method showing the three cuboids fitted to the vertebra point cloud in the axial plane. The same process was also undertaken in the sagittal and coronal planes. In all cases, the cuboids were of equal depth, and the other dimensions were used to define the vertebral measurements. The full list of the measurements taken and their abbreviations is shown.

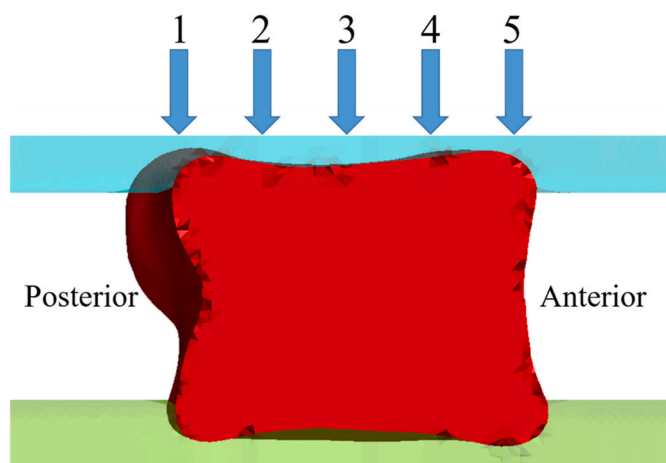


Fig. 3. Locations for the load position sensitivity tests. From posterior (negative) to anterior (positive), the positions relative to the centre were: 1: -20 mm (corresponding with the posterior cortical wall), 2: -10 mm, 3: central loading point, 4: 10 mm and 5: 20 mm (corresponding with the anterior cortical wall).

Table 3
Variation captured in the first five principal components.

Principal Component	Percentage of Variance	Cumulative percentage of Variance
1	29.95	29.95
2	14.33	44.28
3	12.29	56.56
4	9.22	65.78
5	5.91	71.69

3.1. Comparisons of the generated model set to the input set

3.1.1. Geometry

The geometry was compared using the modes of variation described in Table 2. The volume difference between the mean of the input set and mean generated model was 10% (39500 mm³ and 38245 mm³ respectively). The range of vertebral volumes for the input set was 31189 mm³ to 56003 mm³ and for the generated set was 28152 mm³ to 50462 mm³.

There was a strong agreement between the geometric measurements

of the input set and the generated models (Fig. 4), with the means of the two sets agreeing closely. The range of the measurements was also found to be comparable.

3.1.2. Greyscale appearance

The mean greyscale value of each model provides a measure of the specimen's overall bone density. The generated model set (Table 2) broadly replicated the distribution of the vertebral body densities seen in the input set, with a shift to the lower end of the scale (input set range 78–164, mean 108; generated set range 72–122, mean 97).

The greyscale maps in the models generated through the SSAM process captured fewer fine bony features, but retained structures such as the cortical shell region and the vascular channel, although with reduced contrast (Fig. 5D and E). The overall reduction in contrast can be seen in histograms representing the greyscale differences between generated models and the input set (Fig. 5, A-C), where primary deviations are at the high and low greyscale values. This normalised data shows a general agreement in the shape of the curves and the relative quantities between model sets and across the first three principal components.

3.1.3. Stiffness

The mean stiffness of the finite element models of the input set was 4508 N/mm (range 2791 N/mm to 6039 N/mm) and of the generated set (Table 2) was 4134 N/mm (range 2887 N/mm to 6172 N/mm). Results for the first three principal components in isolation are shown in Fig. 6.

3.2. Geometric and bone density variation

The shape of the vertebrae varied substantially within the first three principal components, between the positive and negative standard deviations. The geometric variation in the mid-slices through the anatomical planes can be seen in Fig. 7. Only the +3, the mean and the -3 standard deviations of the principal components are shown, allowing clear visualisation of the main mode of variation present in each principal component; intermediate standard deviation models fitted between these and the mean.

Principal Component 1 contained the least amount of geometric variation within the first three principal components. The vertebral shapes were similar throughout the standard deviations away from the mean, which was especially evident in the axial mid slices. The change in total vertebral volume was limited to 17% larger and 15% smaller

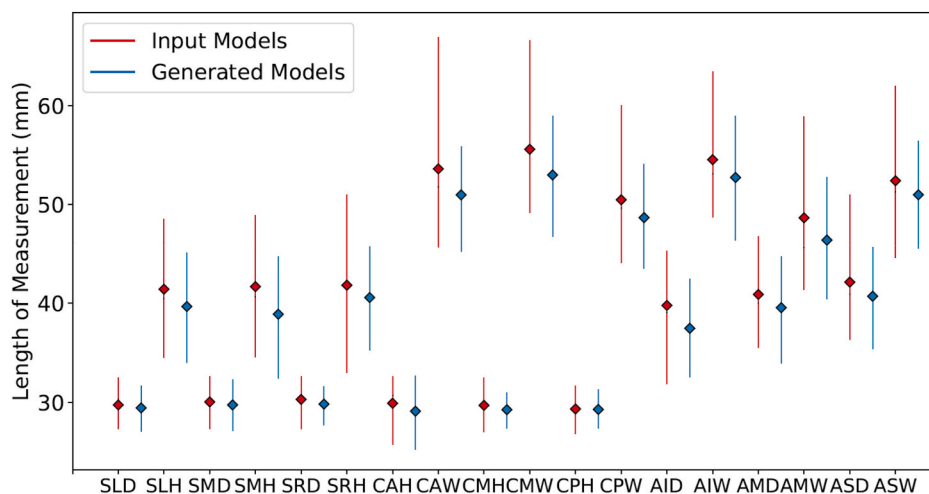


Fig. 4. The variation in the 18 geometric measures (Fig. 2) of the input set models compared to the variation in the generated models for the first three principal components including all combinations of the +1, mean and -1 standard deviations. The range in the measurement is shown by the line and the mean value is shown by the diamond.

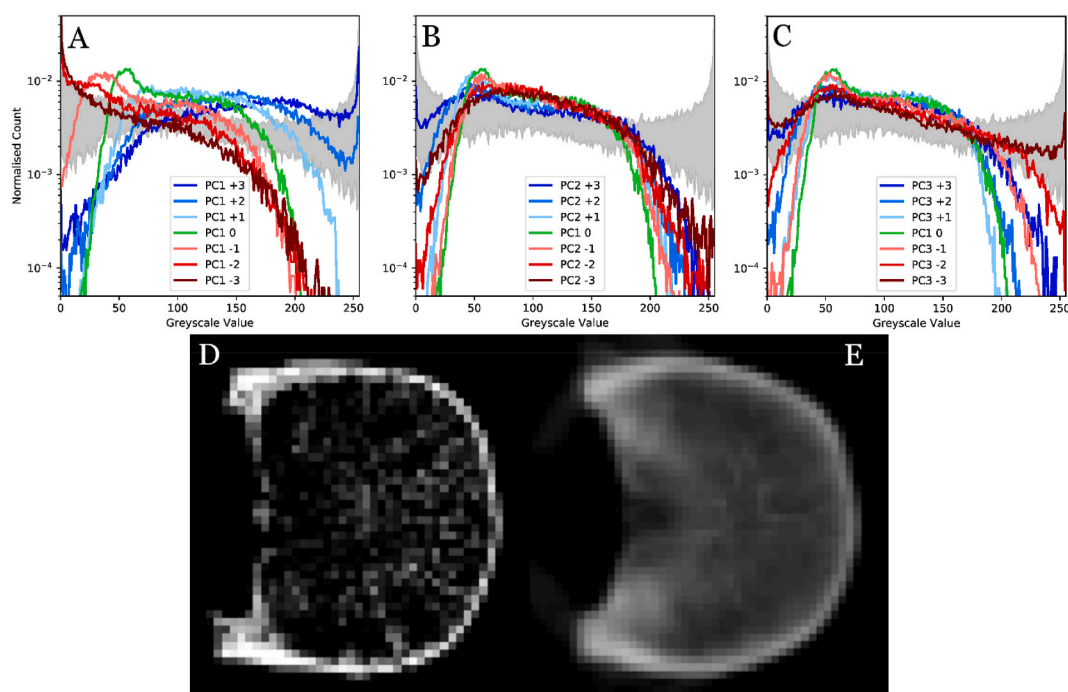


Fig. 5. A–C: Histogram of the models generated from Principal Component 1, 2 and 3 (A, B and C, respectively), with ± 3 , 2 & 1 standard deviations away from the mean. The values are normalised with respect to the total volume of the vertebrae, allowing comparisons with different sized model. The grey background represents the range of histograms seen in the input set. D and E: grayscale backgrounds for the axial mid-slice from the Spine 1 L1 input vertebra (D) and the mean generated model (E).

than the mean model at either end of the standard deviation spectrum.

Principal Component 2 showed the widest geometric variation with many of the different shapes of the input set clearly visible. The large changes to the axial mid slice of the second principal component appear to represent the different levels of the lumbar spine that made up the input set. Positive standard deviations away from the mean had the much wider posterior portion aligning with that of the L5 lumbar vertebrae. Conversely the much narrower -3 S.D. model appeared similar to the L1 lumbar vertebrae. This change in width between the +3 and -3 S.D. was especially evident in the coronal views. The change from L5-like to L1-like vertebrae was also reflected in the sagittal views (Fig. 7) where anterior and posterior wedge shapes were seen in the +3

and -3 S.D. models respectively.

In PC 3, the apparent mode of geometric variation was volume, with the -3 S.D. being 54% larger than the mean and the +3 SD model being 40% smaller than the mean.

Variation in the mean greyscale was almost completely isolated to PC1, with small amounts of variation in PC2 and PC3 (Fig. 6, A). Despite the similarity in the mean greyscale value for PC2 and PC3, the distribution of greyscale values within the bone varied significantly, (Fig. 8). In both PC2 and PC3 the density distribution shifts from the posterior to the anterior of the vertebral body. In PC2 the anterior-posterior shift is alongside a change in shape from L1-like to L5-like. In PC3 the shift of the densest part is from posterior to anterior alongside a reduction in

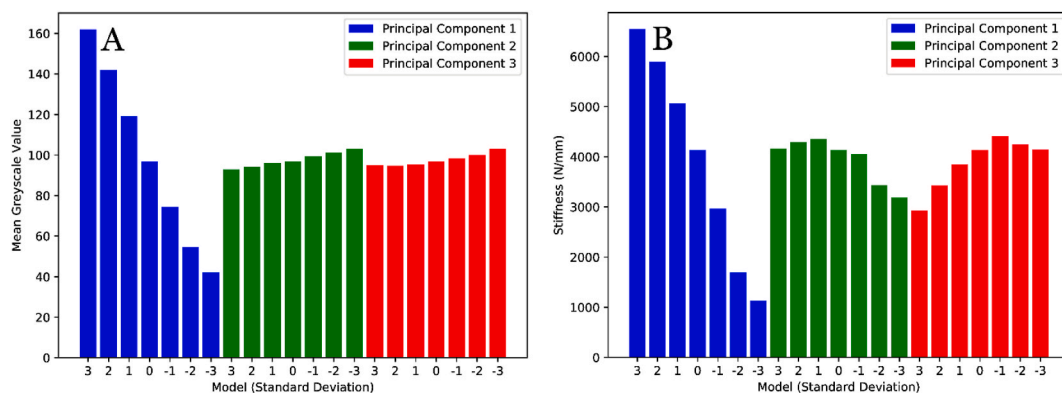


Fig. 6. The mean greyscale (A) and stiffness (B) variation for the first three principal components, including the variation at ± 1 , 2 & 3 standard deviations away from the mean and including the mean.

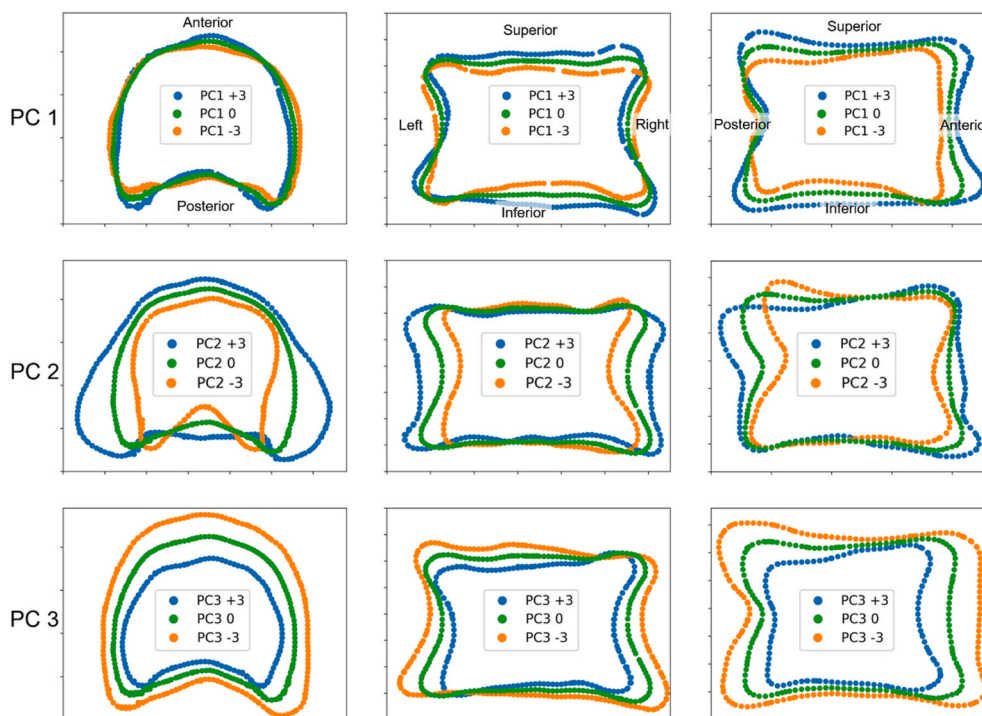


Fig. 7. Axial, coronal and sagittal views of the mid slice of the vertebral models from the first three principal components, showing the mean, +3 and -3 standard deviations away from the mean.

vertebral body volume.

3.3. Stiffness and loading sensitivity

The variation in the resulting stiffness of the generated models is presented in Fig. 6, B. The trends within the different principal components match closely with the variation seen in the mean greyscale (Fig. 6, A).

In the mean generated model, the stiffness was greatest when it was loaded centrally, reducing as loads were applied at greater distances from the centre, with posterior loads yielding slightly higher stiffness values than anterior loads (Fig. 9). Since PC1 primarily affects mean bone density, which is correlated with stiffness (Fig. 6), an overall change in stiffness is seen for that component, without a change in anterior-posterior pattern (Fig. 8). The reduction in stiffness at 20 mm away from the centre, both posteriorly and anteriorly, was proportional to the stiffness when loaded centrally, with reductions of approximately 70% for all standard deviations from the mean. The shape changes

represented by PC2 do not substantially change the stiffness pattern seen in the mean model.

When PC3 was varied, much higher stiffness values were recorded under posterior loading in some cases. Those cases represent larger vertebrae with higher density in the posterior region.

4. Discussion

The objectives of this study were to examine the use of a SSAM to build image-based finite element models of spinal vertebrae and compare the outcomes to specimen-specific finite element models built from the same dataset of 14 lumbar vertebrae. The SSAM was able to generate a range of vertebral models that compared well against the size, shape and density variation found within the input set. The effect of this variation on the response to loading was investigated, showing that the shape and bone density of the vertebral models had large effects on the resultant stiffness. These results encapsulate the main benefits of using a SSAM, over using the original input specimens, for any treatment

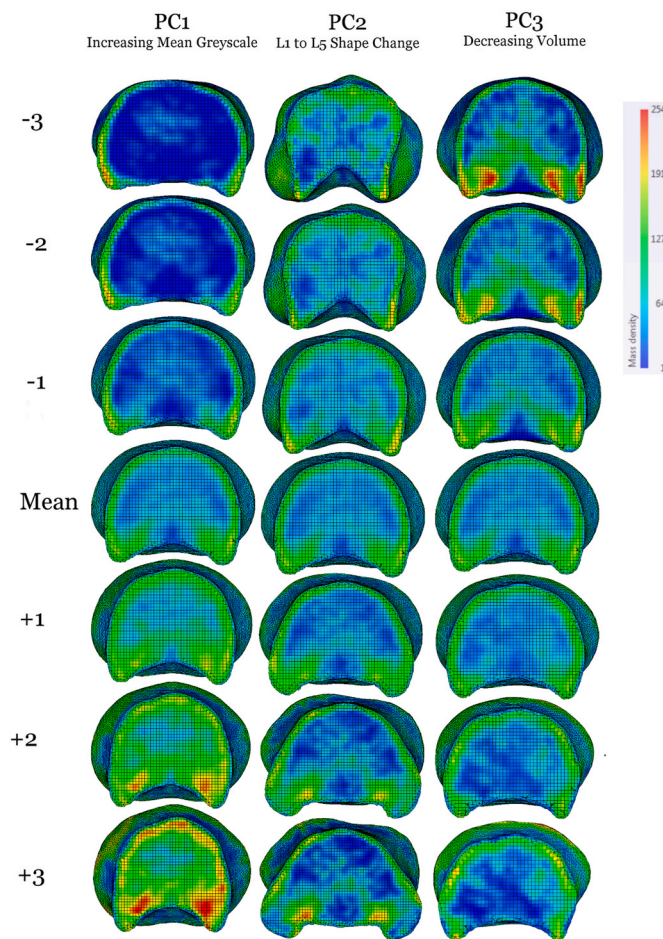


Fig. 8. The variation in the greyscale distribution across the mid-slice of the vertebrae generated from PC1, PC2 and PC3, for each of the $\pm 1, 2$ and 3 standard deviations from the mean. Showing how the changing distribution of the greyscale, even for PC2 and PC3 where the mean greyscale variation is minimal. Red colours indicate denser bone and blue colours indicate the least dense bone.

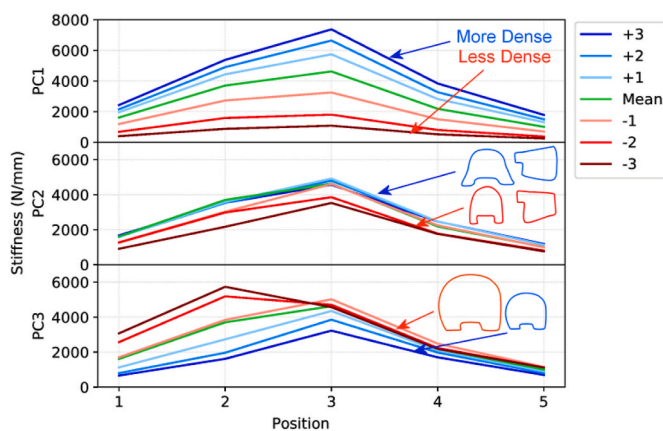


Fig. 9. Effect of loading position on the vertebral stiffness for PC1, PC2 and PC3 from posterior to anterior loading points. Loading point 1 and 2 are 20 mm and 10 mm posterior of the central loading point respectively, loading point 3 is the central position and load points 4 and 5 are 10 mm and 20 mm anterior, respectively. Annotations describe the main modes of variation found in each PC.

investigations. Firstly, we can understand what the main modes of variation are and secondly, we have the ability to generate test cases which combine these variations in controllable ways, while maintaining other associated features. For example, an investigation into the extremes of wedge shapes and vertebral body density could be investigated by combining the extreme standard deviations of PC1 and PC2. While this could be possible without the SSAM, it is unlikely that the variation could be examined with the same level of granularity, or that an accurate distribution of density through the vertebral bodies would be achieved.

Wedge shapes are often an indication of a wedge fracture (Eastell et al., 1991) and therefore this was an important mode of variation to capture due to their prevalence in the target demographic of many vertebral treatments. General shape changes, between L1-like and L5-like vertebrae were also an important mode of variation to capture, given that the input set included vertebrae from these levels. The range of variation within 1 SD (across all possible combinations of the PC1, 2 and 3) was found to capture most of the variation seen in the input set for all measurements taken, including anterior and posterior wedge shapes. In a few cases, models produced variation that was not seen in the experimental input set. Potentially with a larger and therefore more varied input set, such variation may be seen in the input models.

Models used in the remaining investigations were from principal components in isolation, with geometric measurements all falling within the range of the input set. In addition to the range being well represented, the measurements of the mean generated model aligned closely with the mean of the input set measurements, suggesting that the models were not skewed to one end of the variation spectrum. Despite the limited size of the population presented here, measurements agree well with similar measurements recorded in the literature. The mean of the input set vertebral body depth (AID), width (AMW) and height (CPH) was within 14%, 4% and 14% respectively of Wolf et al. (2001) and 11%, 2% and 3% of Hollenbeck et al. (2018) for the comparable measures. Other studies have found geometric distortion at ± 3 standard deviations from the mean (Ali et al., 2012). In this study, no such effects were seen for both shape and density distribution, despite treating the L1 to L5 vertebrae of the input set as continuous.

Comparisons of the density distribution of the models showed that the mean generated greyscale across the vertebral volume matched closely with the greyscale of the input set. The generated greyscale backgrounds lacked only in contrast and definition of the trabecular structure. This means that the micro level trabecular structure was lost, but more macro density regions persist. A clear definition of the cortical shell was visible on all of the generated models, both when the mean density was high and low. This is an important feature of the SSAM, given the importance of the cortical shell in load transfer (Eswaran et al., 2005). This approach to bone density incorporation into the models is particularly important for bones such as vertebrae that have a high proportion of trabecular bone, while approaches that consider cortical and trabecular bone as separate components (Lu and Untaroiu, 2013) may be better suited to long bones. Overall, the density was well represented with comparable mean density of the input set and generated models, suggesting that the method is appropriate. The stiffness of the models is of interest for many clinical treatments and dependent on the density and the shape of the vertebrae (Belkoff et al., 2001; Liebschner et al., 2001; Crawford et al., 2003; Roux et al., 2013). Despite the reduced contrast and accuracy in the density distribution of the generated models, enough information is captured to accurately represent the linear loading behaviour in terms of mean stiffness and the range throughout the generated models.

PC1 described the largest part of the variation and can be characterised as a description of the density variation. This density variation changed both the mean density and the distribution within the vertebral body, as seen in the colour maps, Fig. 8. Of all the variation, changes to the density had the largest effect on the stiffness of the vertebrae, with a variation of ~ 5000 N/mm between most and least stiff. While the

change in mean density varied linearly across the principal components, the resulting stiffness did not. The resulting stiffness appeared to reach a plateau at both +3 and -3 standard deviations from the mean (Fig. 6, B), suggesting that the density distribution (not just the mean density) and minor shape changes have a role in the overall stiffness, given that the volume change is also linear.

L1-like vertebral shapes at the negative standard deviations and L5-like vertebral shapes at the positive standard deviations were measured in PC2. More specifically, the negative standard deviations were much narrower and had a much smaller axial and coronal cross sectional area. Sagittal views of the negative standard deviation models show an anterior wedge shape, mimicking the shape of the most superior lumbar vertebra. The positive standard deviations had a posterior wedge shape, again mimicking the shape of the most inferior lumbar vertebra, following the inflection of the spinal curvature at L3. This agrees with the shapes seen in the input set (Fig. 10) and with results discussed in the literature (Hollenbeck et al., 2018; Wolf et al., 2001; Edmondston et al., 1994; Masharawi et al., 2008; Manohar et al., 1992) where opposing wedge shapes exist either side of the L3 vertebra. The continuous nature of the lumbar section of the spine is what allows the use of input specimens from the entire section. The consequence of this is that it allows for the identification of both gradual shape changes between levels and the changing density distribution. Additionally, it provides a method of creating level-matched vertebrae for functional unit models. These multi-level models are vital for applications in the examination of disc replacement and vertebral fixation.

The sensitivity of the SSAM models to loading position was examined because the resulting stiffness is affected by both the shape and density distribution across the whole vertebra. It is therefore a good measure of the resultant mechanical consequences of the variation. The response to loading the mean model was similar to that seen with the input set and to results seen in the literature (Robson Brown et al., 2014), with reductions in stiffness greater to the anterior. The increase in stiffness when loaded posteriorly in the study by Robson Brown et al. (Robson Brown et al., 2014) was not recorded here due to the absence of the posterior elements in these models. Within PC1, the variation followed expectations, given the incremental change in the mean density. The outliers in PC2, the -1, -2 and -3 S.D. models, showed a reduced posterior density and hence showed a reduced stiffness when loaded posteriorly.

The main limitation of the study is the limited and biased input set. This was biased towards the elderly population and the upper end of the lumbar section, the results, therefore, cannot be applied to the population in general. However, this study does provide a proof of concept for the incorporation of material and shape changes in a single model. Expansion of the input data would allow for investigations into age and sex differences, and the potential to include multiple time points would enable the osteoarthritic progression to be examined, akin to Barr et al. (2016). A larger input set also permits the testing of the model

robustness through testing of the specificity, generality, and compactness.

Previous studies have commented on the changing mean density through spinal level (Edmondston et al., 1994; Steiger et al., 1990) where density generally reduces through the lumbar sections, attributed to the changing vertebral shape. The density variation within vertebrae (anterior/superior/posterior/inferior) has also been investigated (Hulme et al., 2007), however the variability at different levels was not reported. The shifting density distribution, a feature difficult to identify experimentally, could be due to the bone response to varying load distribution at different levels, which can be complicated further with the amount of lumbar lordosis (Bruno et al., 2017). This tool could incorporate those studies that have identified the variation in lordosis and kyphosis through SSMs (Ali et al., 2012; Meakin et al., 2009; Boisvert et al., 2008) to investigate the relationships between spinal level, spinal curvature and vertebral density distributions.

5. Conclusion

The variation captured in the models shows that the methodology presents an option for generating controllable datasets of vertebral body models for identifying the response to various treatments. The links between shape and density distribution are particularly useful due to the dependence on the internal bone structure on the response to load bearing and subsidence of intervertebral devices. The methodology used is unique to sections of the spine, where variation level to level can be treated as continuous, allowing a mix of vertebral levels to be used in the same shape and appearance model. The SSAM methodology applied in this study was shown to be able to accurately capture and describe the variation found in the vertebral image input set, allowing, for example, devices to be tested over a range of realistic shape variations. Finite element models of the vertebrae generated show a behaviour similar to the input set with the mean and range of variation well represented. The integrated approach of including shape and material property variation within the SSAM presents a new method to find modes of variation that are difficult to identify through other means and provide a way to investigate and optimise treatments across a patient population.

Funding

This work was supported by the European Research Council (2012-StG-306615), Engineering and Physical Sciences Research Council (EP/L014823/1) and Innovation and Knowledge Centre (EP/I019103/1).

Ethics

Cadaveric spines were obtained with ethical permission from the Leeds GIFT Research Tissue Project and reviewed by NHS Research Ethics Committee reference 15/YH/0096.

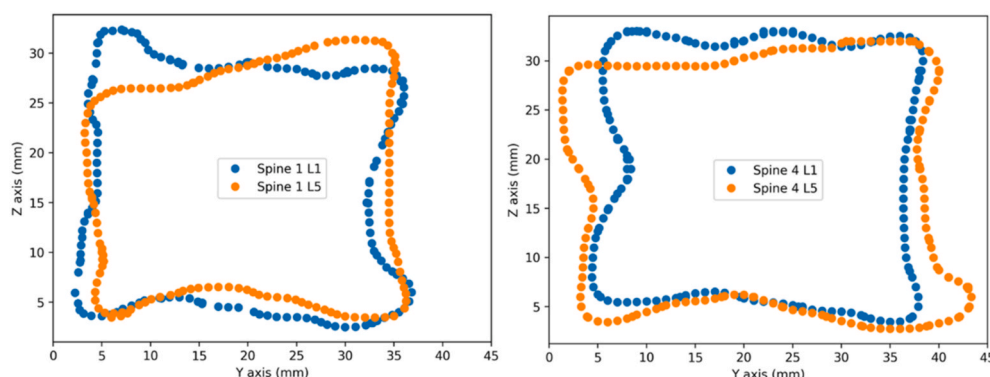


Fig. 10. Sagittal views of the L1 and L5 vertebrae from spine 1 and spine 4 of the input set, showing the opposing wedge shapes of the two.

Data

The data set associated with this paper is openly available from the University of Leeds data repository (Day et al., 2021).

CRedit authorship contribution statement

G.A. Day: Conceptualization, Methodology, Software, Validation, Formal analysis, Investigation, Data curation, Writing – original draft, Writing – review & editing, Visualization. **A.C. Jones:** Conceptualization, Writing – review & editing, Visualization, Supervision, Project administration. **R.K. Wilcox:** Conceptualization, Writing – review & editing, Visualization, Supervision, Project administration, Funding acquisition.

Declaration of competing interest

The authors declare that they have no known competing financial interests or personal relationships that could have appeared to influence the work reported in this paper.

References

- Ali, A.H.A., Cowan, A.B., Gregory, J.S., Aspden, R.M., Meakin, J.R., 2012. The accuracy of active shape modelling and end-plate measurements for characterising the shape of the lumbar spine in the sagittal plane. *Comput. Methods Biomech. Biomed. Eng.* 15, 167–172. <https://doi.org/10.1080/10255842.2010.518962>.
- Aquarius, R., Homminga, J., Hosman, A.J.F., Verdonchot, N., Tanck, E., 2014. Prophylactic vertebroplasty can decrease the fracture risk of adjacent vertebrae: an in vitro cadaveric study. *Med. Eng. Phys.* <https://doi.org/10.1016/j.medengphy.2014.03.009>.
- Barr, A.J., Dube, B., Hensor, E.M.A., Kingsbury, S.R., Peat, G., Bowes, M.A., Sharples, L. D., Conaghan, P.G., 2016. The relationship between three-dimensional knee MRI bone shape and total knee replacement—a case control study: data from the Osteoarthritis Initiative. *Rheumatology* 55, 1585–1593. <https://doi.org/10.1093/rheumatology/kew191>.
- Belkoff, S.M., Mathis, J.M., Jasper, L.E., 2001. The biomechanics of vertebroplasty. *Spine* 26, 1537–1541. <https://doi.org/10.1097/00007632-200107150-00007>.
- Boisvert, J., Cheriet, F., Pennec, X., Labelle, H., Ayache, N., 2008. Geometric variability of the scoliotic spine using statistics on articulated shape models. *IEEE Trans. Med. Imag.* 27, 557–568. <https://doi.org/10.1109/TMI.2007.911474>.
- Bredbenner, T.L., Eliason, T.D., Francis, W.L., McFarland, J.M., Merkle, A.C., Nicoletta, D.P., 2014. Development and validation of a statistical shape modeling-based finite element model of the cervical spine under low-level multiple direction loading conditions. *Front. Bioeng. Biotechnol.* 2 <https://doi.org/10.3389/fbioe.2014.00058>.
- Bruno, A.G., Burkhart, K., Allaire, B., Anderson, D.E., Boussein, M.L., 2017. Spinal loading patterns from biomechanical modeling explain the high incidence of vertebral fractures in the thoracolumbar region. *J. Bone Miner. Res.* 32, 1282–1290. <https://doi.org/10.1002/jbmr.3113>.
- Bryan, R., Surya Mohan, P., Hopkins, A., Galloway, F., Taylor, M., Nair, P.B., 2010. Statistical modelling of the whole human femur incorporating geometric and material properties. *Med. Eng. Phys.* 32, 57–65. <https://doi.org/10.1016/j.medengphy.2009.10.008>.
- Campbell, J.Q., Petrella, A.J., 2015. An automated method for landmark identification and finite-element modeling of the lumbar spine. *IEEE (Inst. Electr. Electron. Eng.) Trans. Biomed. Eng.* 62, 2709–2716. <https://doi.org/10.1109/TBME.2015.2444811>.
- Campbell, J.Q., Petrella, A.J., 2016. Automated finite element modeling of the lumbar spine: using a statistical shape model to generate a virtual population of models. *J. Biomech.* 49, 2593–2599. <https://doi.org/10.1016/j.jbiomech.2016.05.013>.
- Clogenson, M., Duff, J.M., Luethi, M., Levivier, M., Meuli, R., Baur, C., Henein, S., 2015. A statistical shape model of the human second cervical vertebra. *Int. J. Comput. Ass. Radiol. Surg.* 10, 1097–1107. <https://doi.org/10.1007/s11548-014-1121-x>.
- Crawford, R.P., Cann, C.E., Keaveny, T.M., 2003. Finite element models predict in vitro vertebral body compressive strength better than quantitative computed tomography. *Bone* 33, 744–750. [https://doi.org/10.1016/S8756-3282\(03\)00210-2](https://doi.org/10.1016/S8756-3282(03)00210-2).
- Dagenais, S., Caro, J., Haldeman, S., 2008. A systematic review of low back pain cost of illness studies in the United States and internationally. *Spine J.* 8, 8–20. <https://doi.org/10.1016/j.spinee.2007.10.005>.
- Day, G.A., Jones, A.C., Wilcox, R.K., 2020. Optimizing computational methods of modeling vertebroplasty in experimentally augmented human lumbar vertebrae. *JOR SPINE* 3. <https://doi.org/10.1002/jsp2.1077>.
- Day, G. A. and Jones, A. C. and Wilcox, R. K. (2021) Dataset associated with 'Using Statistical Shape and Appearance Modelling to characterise the 3D shape and material properties of human lumbar vertebrae: A proof of concept study'. University of Leeds. [Dataset] <https://doi.org/10.5518/874>.
- De Beer, N., Scheffer, C., 2012. Reducing subsidence risk by using rapid manufactured patient-specific intervertebral disc implants. *Spine J.* 12, 1060–1066. <https://doi.org/10.1016/j.spinee.2012.10.003>.
- Eastell, R., Cedel, S.L., Wahner, H.W., Riggs, B.L., Melton, L.J., 1991. Classification of vertebral fractures. *J. Bone Miner. Res.* 6, 207–215. <https://doi.org/10.1002/jbmr.5650060302>.
- Edmondston, S.J., Singer, K.P., Price, R.L., Day, R.E., Bredahl, P.D., 1994. The relationship between bone mineral density, vertebral body shape and spinal curvature in the elderly thoracolumbar spine: an in vitro study. *Br. J. Radiol.* 67, 969–975. <https://doi.org/10.1259/0007-1285-67-802-969>.
- Eswaran, S.K., Gupta, A., Adams, M.F., Keaveny, T.M., 2005. Cortical and trabecular load sharing in the human vertebral body. *J. Bone Miner. Res.* 21, 307–314. <https://doi.org/10.1359/jbmr.2006.21.2.307>.
- Grassi, L., Schileo, E., Boichon, C., Viceconti, M., Taddei, F., 2014. Comprehensive evaluation of PCA-based finite element modelling of the human femur. *Med. Eng. Phys.* 36, 1246–1252. <https://doi.org/10.1016/j.medengphy.2014.06.021>.
- Hasegawa, T., et al., 2020. The titanium-coated PEEK cage maintains better bone fusion with the endplate than the PEEK cage 6 Months after PLIF surgery—a multicenter, prospective, Randomized study. *Spine* 1. <https://doi.org/10.1097/brs.00000000000003464>.
- Hollenbeck, J.F.M., Cain, C.M., Fattor, J.A., Rullkoetter, P.J., Laz, P.J., 2018. Statistical shape modeling characterizes three-dimensional shape and alignment variability in the lumbar spine. *J. Biomech.* 69, 146–155. <https://doi.org/10.1016/j.jbiomech.2018.01.020>.
- Hsu, W.E., Su, K.C., Chen, K.H., Pan, C.C., Lu, W.H., Lee, C.H., 2019. The evaluation of different radiological measurement parameters of the degree of collapse of the vertebral body in vertebral compression fractures. *Appl. Bionics Biomechanics* 2019. <https://doi.org/10.1155/2019/4021640>.
- Hulme, P.A., Boyd, S.K., Ferguson, S.J., 2007. Regional variation in vertebral bone morphology and its contribution to vertebral fracture strength. *Bone* 41, 946–957. <https://doi.org/10.1016/j.bone.2007.08.019>.
- Hurwitz, E.L., Randhawa, K., Yu, H., Côté, P., Haldeman, S., 2018. The Global Spine Care Initiative: a summary of the global burden of low back and neck pain studies. *Eur. Spine J.* 27, 796–801. <https://doi.org/10.1007/s00586-017-5432-9>.
- Liebschner, M.A., Rosenberg, W.S., Keaveny, T.M., 2001. Effects of bone cement volume and distribution on vertebral stiffness after vertebroplasty. *Spine* 26, 1547–1554. <https://doi.org/10.1097/00007632-200107150-00009>.
- Lu, Y.C., Untaroiu, C.D., 2013. Statistical shape analysis of clavicular cortical bone with applications to the development of mean and boundary shape models. *Comput. Methods Progr. Biomed.* 111, 613–628. <https://doi.org/10.1016/j.cmpb.2013.05.017>.
- Manohar, P.M., Goel, V., Oxland, T., Takata, K., Duranceau, J., Krag, M., Price, M., 1992. Human lumbar vertebrae: quantitative three-dimensional anatomy. *Spine* 17, 299–306. <https://doi.org/10.1097/00007632-199203000-00010>.
- Masharawi, Y., Salame, K., Mirovsky, Y., Peleg, S., Dar, G., Steinberg, N., Hershkovitz, I., 2008. Vertebral body shape variation in the thoracic and lumbar spine: characterization of its asymmetry and wedging. *Clin. Anat.* 21, 46–54. <https://doi.org/10.1002/ca.20532>.
- McCormack, T., Karaikovic, E., Gaines, R.W., 1994. The load sharing classification of spine fractures. *Spine* 19, 1741–1744. <https://doi.org/10.1097/00007632-199408000-00014>.
- McCormick, M., Liu, X., Jomier, J., Marion, C., Ibanez, L., 2014. ITK: enabling reproducible research and open science. *Front. Neuroinf.* 8, 13. <https://doi.org/10.3389/fninf.2014.00013>.
- Meakin, J.R., Gregory, J.S., Aspden, R.M., Smith, F.W., Gilbert, F.J., 2009. The intrinsic shape of the human lumbar spine in the supine, standing and sitting postures: characterization using an active shape model. *J. Anat.* 215, 206–211. <https://doi.org/10.1111/j.1469-7580.2009.01102.x>.
- Meakin, J.R., Fulford, J., Seymour, R., Welsman, J.R., Knapp, K.M., 2013. The relationship between sagittal curvature and extensor muscle volume in the lumbar spine. *J. Anat.* 222, 608–614. <https://doi.org/10.1111/joa.12047>.
- Meller, S., Kalender, W.A., 2004. Building a statistical shape model of the pelvis. *Int. Congr.* 1268, 561–566. <https://doi.org/10.1016/j.ics.2004.03.295>.
- Mengoni, M., 2017. opt4Abq (v 2.0), a generic python code to run Abaqus in an optimisation loop. See <https://doi.org/10.5281/zenodo.580475>.
- Mengoni, M., Luxmoore, B.J., Wijayathunga, V.N., Jones, A.C., Broom, N.D., Wilcox, R. K., 2015. Derivation of inter-lamellar behaviour of the intervertebral disc annulus. *J. Mech. Behav. Biomed. Mater.* 48, 164–172. <https://doi.org/10.1016/j.jmbm.2015.03.028>.
- Nicoletta, D.P., Bredbenner, T.L., 2012. Development of a parametric finite element model of the proximal femur using statistical shape and density modelling. *Comput. Methods Biomech. Biomed. Eng.* 15, 101–110. <https://doi.org/10.1080/10255842.2010.515984>.
- Robson Brown, K., Tarsuslugil, S., Wijayathunga, V.N., Wilcox, R.K., 2014. Comparative finite-element analysis: a single computational modelling method can estimate the mechanical properties of porcine and human vertebrae. *J. R. Soc. Interface/the Royal Society* 11, 20140186. <https://doi.org/10.1098/rsif.2014.0186>.
- Roux, J.P., Wegrzyn, J., Boutroy, S., Boussein, M.L., Hans, D., Chapurlat, R., 2013. The predictive value of trabecular bone score (TBS) on whole lumbar vertebrae mechanics: an ex vivo study. *Osteoporos. Int.* 24, 2455–2460. <https://doi.org/10.1007/s00198-013-2316-7>.
- Steiger, P., Block, J.E., Steiger, S., Heuck, A.F., Friedlander, A., Ettinger, B., Harris, S.T., Glüer, C.C., Genant, H.K., 1990. Spinal bone mineral density measured with

- quantitative CT: effect of region of interest, vertebral level, and technique. *Radiology* 175, 537–543. <https://doi.org/10.1148/radiology.175.2.2326479>.
- Wolf, A., Shoham, M., Michael, S., Moshe, R., 2001. Morphometric study of the human lumbar spine for operation-workspace specifications. In: *Spine*, pp. 2472–2477. <https://doi.org/10.1097/00007632-200111150-00015>.
- Yates, K.M., Lu, Y.C., Untaroiu, C.D., 2016. Statistical shape analysis of the human spleen geometry for probabilistic occupant models. *J. Biomech.* 49, 1540–1546. <https://doi.org/10.1016/j.jbiomech.2016.03.027>.